Asian Journal of Chemistry; Vol. 36, No. 8 (2024), 1912-1920

ASIAN JOURNAL OF CHEMISTRY

https://doi.org/10.14233/ajchem.2024.31921

Copper and Nitrogen co-doped ZnO Nanomaterials with Enhanced Photocatalytic and Antibacterial Activities

MOHAMMED HUMAYUN RASHID CHOUDHURY[1], MD NIZAM UDDIN[1,*], PARTHA PRATIM NATH[1], IQBAL AHMED SIDDIQUEY[1], MOHAMMAD RAZAUL KARIM[1], MD. AZHARUL ARAFATH[1], CHINTALAPALLE V. RAMANA[2] and MOHAMMED MUZIBUR RAHMAN[3]

[1]Department of Chemistry, Shahjalal University of Science and Technology, Sylhet-3114, Bangladesh
[2]Center for Advanced Materials Research (CMR), Aerospace & Mechanical Engineering, University of Texas at El Paso, El Paso, TX 79968, USA
[3]Department of Chemistry, King Abdulaziz University, Jeddah 21589, P.O.Box 80203, Saudi Arabia

*Corresponding author: E-mail: nizam3472@yahoo.com; nizam-che@sust.edu

Received: 9 May 2024; *Accepted*: 5 July 2024; *Published online*: 25 July 2024; AJC-21713

This work demonstrates the enhanced photocatalytic and antibacterial activities of copper and nitrogen-co-doped ZnO (Cu-N-ZnO) nanomaterials deposited onto soda-lime glass using a low-cost chemical approach. The effect of combined Cu-N doping is significant on the structure, properties, and performance of ZnO, as revealed from the characterization results. The synthesized materials crystallize in a hexagonal wurtzite structure of ZnO with a high degree of crystallinity, according to X-ray diffraction (XRD) experiments. The scanning electron microscopy (SEM) analysis indicated a uniformly distributed morphology with spherical-like ZnO nanoparticles. The optical studies revealed that the band gap decreases significantly in 5% Cu-5% N co-doped ZnO (2.89 eV) compared to intrinsic ZnO (3.36 eV). The photocatalytic and antibacterial activities of the samples were evaluated by the degradation of methylene blue dye in aqueous media and the inactivation of *E. coli* bacteria under visible light irradiation. The 5% Cu-5% N doped ZnO showed the highest dye degradation efficiency, which was 64.44% higher than that of the intrinsic ZnO and inactivated 62.53% more bacteria in the presence of light compared to that in a dark condition. Moreover, Cu-N co-doped ZnO inactivated 79.06% and 23.22% more bacteria than bare glass slides and ZnO under visible light irradiation, respectively.

Keywords: Copper, ZnO, Doping, Optical properties, Photocatalysis, Antibaterial activity, Methylene blue dye.

INTRODUCTION

Zinc oxide is one of the most significant oxide materials, finds applications in a wide range of technologies, such as energy storage and conversion, transistors, panel displays, photodetectors, sensors and catalysis [1-6]. The application potential of ZnO can be attributed to its typical material properties, which include a direct band gap of 3.37 eV, transparency in the visible light spectrum and a significant exciton binding energy of 60 meV [4-6]. Significantly, ZnO-based photocatalysts have drawn extensive attention due to their exceptional qualities, which include higher chemical stability, better optical and electrical responsiveness, non-toxicity and natural abundance [7-10]. Nevertheless, the quick recombination of photogenerated charge carriers, which significantly lowers the quantum efficiency of photocatalyst, is a significant disadvantage to reaching high photocatalytic efficiency. In addition, the high band gap of ZnO restricts the use of visible light for different applications [11]. Numerous techniques, including semiconductor coupling, noble metal deposition, metal doping, non-metal modification and dye sensitization, have been devised to get around this limitation [12-16].

Typically, doping ZnO with transition and noble metals has been considered an approach to designing photocatalytic materials with functionality in the visible region of the electromagnetic spectrum. Doping ZnO with transition and noble metals generally improves its characteristics by producing lower energy states as it facilitates electron trapping and reduces the band gap [17]. Different research groups have studied various transition metals such as Ti [18], Fe [9,19,20], Ni [21-23], Co [24], Cu [25-29], Mn [30], W [31], Ru [32], Mo [33], V [34] and other metals like Ga [35,36] and Al [37] as dopants. Doping

with lanthanides, particularly Ce [38-41], has also attra-cted a lot of attention. Typically, these dopants are added to the ZnO matrix and take up interstitial or substitution sites [38]. Transition metals have their redox energy states in between the energy bands of semiconductors. Depending on where it is with respect to the valence or conduction band, this acts as a trap for photo-generated electrons or holes [17,42]. On the other hand, there have also been reports of potential drawbacks of transition metal doping, including thermal instability.

The present work was performed on the transition-metal (Cu) and a non-metal (N) co-doped ZnO nanomaterials to enhance its photocatalytic and antibacterial activity. Copper, among several transition metals, has been doped in the ZnO semi-conductor due to a number of intriguing characteristics, for example, copper has a larger ionization energy than zinc and has incorporated the high concentration of impurities as facilitated by the low formation energy of group 11 elements [43]. Moreover, the smaller effective mass, which is indicated by the large coupling between the *p*-orbitals of oxygen and the *d*-orbitals of dopant, enhances electron transport in the lattice [44]. So, a significant modification of the surface as well as the optical properties of ZnO can be affected by Cu doping [17,45]. Along with Cu, we also considered a non-metal, nitrogen, for co-doping into ZnO. It is advantageous to choose nitrogen as a dopant due to a number of its significant characteristics. A few explanations for this doping are that nitrogen atoms can replace oxygen and occupy those sites [46]. Again, nitrogen and oxygen are similar in size and nitrogen has a lower ionization energy than oxygen [42,46]. As seen in N-TiO_2, the presence of nitrogen in the metal oxide's interstitial sites may influence the establishment of sub-bands above the valance band [47]. In case of TiO_2, the band positioning of interband in the substitution doping is lower than that of interstitial doping [48]. Hence, for interstitial doping, electron excitation from a highly occupied level to the conduction band is simpler [17]. Hence, N-doping in ZnO may facilitate band gap modification and enhancement of charge transfer. Therefore, in this study, the Cu- and N co-doping approach were employed to derive the excellent properties and performance in ZnO. Pure ZnO, Cu-doped ZnO and Cu- and N-co-doped ZnO nanomaterials were prepared by a low-cost sol-gel drop coating method for the first time. The photocatalytic and antibacterial activities of these nanostructured thin films were investigated by photodegradation of methylene blue dye and inactivation of *E. coli* bacteria under visible light irradiation. As presented and discussed in this article, the results demonstrate that the Cu- and N-co-doped ZnO materials with optimum composition exhibits enhanced photocatalytic and antibacterial activity and are quite useful for practical applications.

EXPERIMENTAL

Zinc acetate dihydrate (Sigma-Aldrich) and triethanolamine (TEA, Sigma-Aldrich) were used as sources of Zn and stabilizer, respectively. Anhydrous ethanol (VWR Int. Ltd.) was used as a solvent, whereas copper acetate monohydrate (Merck) and urea (Sigma-Aldrich) were used as the sources of copper and nitrogen, respectively. The soda lime silica glass slides were used as substrates for thin film. Chromic acid (Sigma-Aldrich) and dichloromethane (Fisher Scientific) were used for the cleaning of these glass substrates. Nutrient agar (Merck) and NaCl (Sigma-Aldrich) were used for the antibacterial study.

Synthesis of pure, Cu-doped and Cu and N co-doped ZnO nanomaterials: Sol-gel drop coating was utilized to synthesize the nanostructured ZnO thin film. At first, zinc acetate dihydrate was added to 9.6 mL of absolute ethanol by vigorous stirring and then 0.4 mL of TEA was added dropwise to the mixture. The solution was agitated at 200 rpm for 2-3 min, heated at 65 ºC for 1 h, and maintained the volume of 10 mL to obtain a transparent and stable ZnO sol. Then the sol was aged for 24 h and furthermore, it was used for film preparation. The same method was used to prepare Cu-doped ZnO and Cu and N-co-doped ZnO thin films. An appropriate amount of copper acetate monohydrate and urea were added as Cu and N precursors, respectively, to the solution of zinc acetate dihydrate, TEA and ethanol. It was then stirred for 3 min at 200 rpm, heated for 1 h at 65 ºC and then the formed transparent sol was aged for 24 h. To fabricate the sample, soda lime silica glasses with dimensions of 60 mm × 25 mm × 1.5 mm were abrassed by a sand blast machine prior to the coating process. Then the abrasive glasses were washed by using chromic acid and a dichloromethane solution. Finally, alcohol and deionized water were also used to wash the abrasive glass substrates and subsequently dried at 100 ºC. For the preparation of bare ZnO, Cu-doped ZnO and Cu and N co-doped ZnO thin films, 0.2 mL prepared sol was cast dropwise on each abrasive glass substrate uniformly and then heated at 80 ºC for 20 min in an oven. The coating was repeated four times and finally the films were annealed at 500 ºC for 2 h using a muffle furnace (JSMF-30T, Korea).

Characterization: The crystal structure and phase of the Cu-N-ZnO thin films were determined by their XRD pattern using X-rays from a Cu*K*α source. SEM imaging was also used to examine the morphology of the synthesized thin films. The accurate compositions of the samples were verified by using energy dispersive X-ray spectroscopy (EDS) spectra. It also provided information regarding the purity of the samples. For Fourier transform infrared spectroscopy (FTIR) analysis, the samples were taken in a KBr matrix and the spectra were recorded by IRPrestige-21 (Shimadju, Japan). UV-Visible spectroscopy was used to record the absorption spectra of the samples using a UV-1800 spectrophotometer (Shimadju, Japan) and the photoluminescence (PL) spectra were recorded using an RF-5301pc spectroflurophotometer (Shimadzu, Japan).

Photocatalytic activity: In order to assess the photocatalytic activity of the synthesized nanocomposites, 250 mL of 5 ppm methylene blue dye (Merck) were photodegraded for 240 min in a visible light chamber. A 200 W tungsten lamp was used as a light source in the visible chamber. To achieve the adsorption-desorption equilibrium, the sample film was dipped in the dye solution and left in dark for 30 min for each study. Throughout the experiment, the solution was magnetically stirred and a constant temperature of 25 ºC was maintained by a cyclic flow of cooling water using a refrigerating bath circulator (RW-0525G, Lab Companion). The tungsten

lamp was kept 25 cm above the dye solution's surface. The methylene blue dye solution (3 mL) was pipetted out of the beaker once every 30 min and the absorption data of dye solution was recorded by a UV-Vis spectrophotometer accordingly. Considering the maximum absorbance at 664 nm, the degradation efficiency was computed using eqn. 1:

$$\text{Efficiency } (\%) = \frac{C_o - C_t}{C_o} \times 100 \approx \frac{A_o - A_t}{A_o} \times 100 \quad (1)$$

In this case, C_o and C_t represented the initial concentration of dye, the reduced concentration of dye at time (t) and whereas, A_o and A_t were the initial absorbance and absorbance at time t, respectively. By using the data of dye degradation with time, the $C_t - C_o$ *vs.* time and log (C_t/C_o) *vs.* time curves were plotted to study the zero-order and first-order kinetics, respectively. The rate of reaction and regression coefficient (R^2) for both orders were calculated from the graph by using eqns. 2 and 3, respectively [49]:

For zero-order kinetics:

$$C_t - C_o = -kt \quad (2)$$

For first-order kinetics:

$$\log \frac{C_t}{C_o} = -kt \quad (3)$$

Antibacterial activity: The antibacterial study of the thin films was carried out by the simple drop test method [49]. For the antibacterial study, all the apparatus was sterilized at 120 ºC and 3 atm pressure in the autoclave for 30 min. Then the apparatus was dried and treated under UV radiation. For the preparation of the agar bed, 1 g of nutrient agar was dissolved in a 100 mL solution and sterilized at 120 ºC and 3 atm in an autoclave for 15 min. Then, it was cooled to 50 ºC and 10 mL of solution was placed on each Petri dish. To check the antibacterial activity, 250 µL of 1.5 × 10^8 CFU/mL bacterial solution was cast on the 25 mm × 25 mm sample film. The sample film was then irradiated under tungsten light (at a distance of 25 cm) for 1 h. At the same time, another identical solution was kept in dark for the same time period for comparison. After 1 h, each film was washed with 16 mL of distilled water and the mixture was then diluted 30 times and 10 µL of this solution was spread on the prepared agar bed in a petri dish. Then the dishes were placed in an incubator at 37 ºC for 24 h. After 24 h of incubation, the number of colonies that survived was counted and photographs of the petri dishes were taken. This process was repeated for each sample. A similar experiment was conducted on a bare glass slide of the same dimension (blank solution) for proper comparison.

RESULTS AND DISCUSSION

XRD studies: The XRD patterns of the synthesized thin films are shown in Fig. 1. All the sharp and strong peaks present in the XRD spectra represent the existence of pure hexagonal phase of wurtzite-type ZnO. The planes (1 0 0), (0 0 2), (1 0 1), (1 0 2), (1 1 0), (1 0 3), (2 0 0), (1 1 2), (2 0 1), (0 0 4) and (2 0 2) are represented by the strong peaks at angles (2θ) of 31.7º, 35.8º, 38.8º, 45.6º, 48.8º, 56.6º, 61.5º, 66.5º, 68.3º, 72.6º and 75.5º, respectively, which are all in accordance with JCPDS card no. 36-1451 [7,16,50-52]. The diffraction peaks are sharp and intense, exhibiting the high crystallinity of the samples, while there is no evidence of the presence of other phases. The absence of any secondary phases is a confirmation of the phase purity of all the materials synthesized. The Scherrer's equation (eqn. 4) was utilized to determine the average size of the crystallites (D) using the XRD data, in addition to identifying the crystalline phase:

$$D = \frac{k\lambda}{\beta \cos\theta} \quad (4)$$

where the X-ray wavelength of Cu*K*α is represented by λ = 0.15405 nm, k = 0.9, the full-width at half-maximum intensity (FWHM) in radians is represented by β and the peak's Bragg angle is shown by θ. The calculated average crystal size is shown in Table-1.

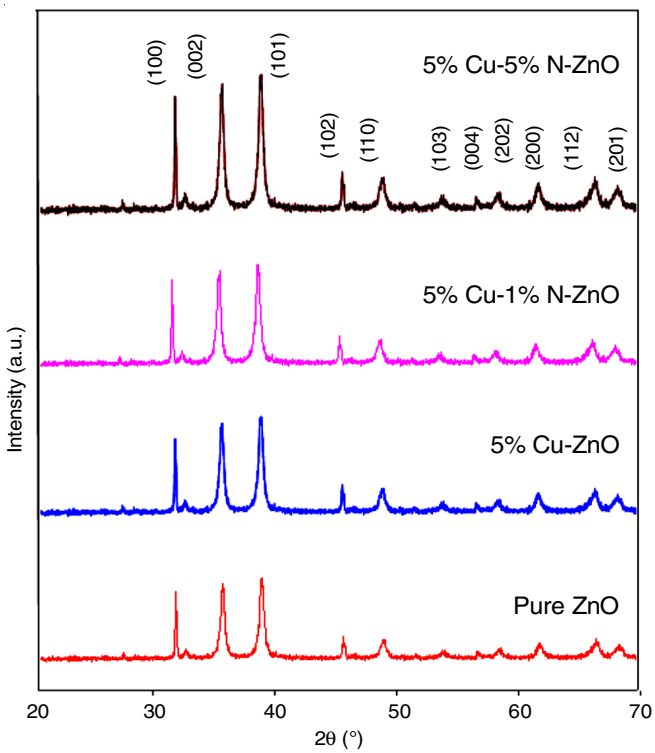

Fig. 1. XRD patterns of pure ZnO, 5% Cu-ZnO, 5% Cu-1% N-ZnO and 5%Cu-5%N-ZnO. The indexing of the patterns indicate that all the materials crystallize in wurtzite-type ZnO

TABLE-1
AVERAGE CRYSTALLITE SIZE OF THE PRODUCED SAMPLES CALCULATED BY SCHERRER'S EQUATION

Samples	Average crystallite size (nm)
Pure ZnO	29.2
5% Cu-ZnO	31.4
5% Cu-1% N-ZnO	31.7
5% Cu-5% N-ZnO	34.0

SEM studies: The SEM images of pure ZnO thin film with different magnifications are shown in Fig. 2. The images indicated that the thin film consists of relatively spherical-shaped agglomerates of ZnO nanoparticles. In addition, the film has

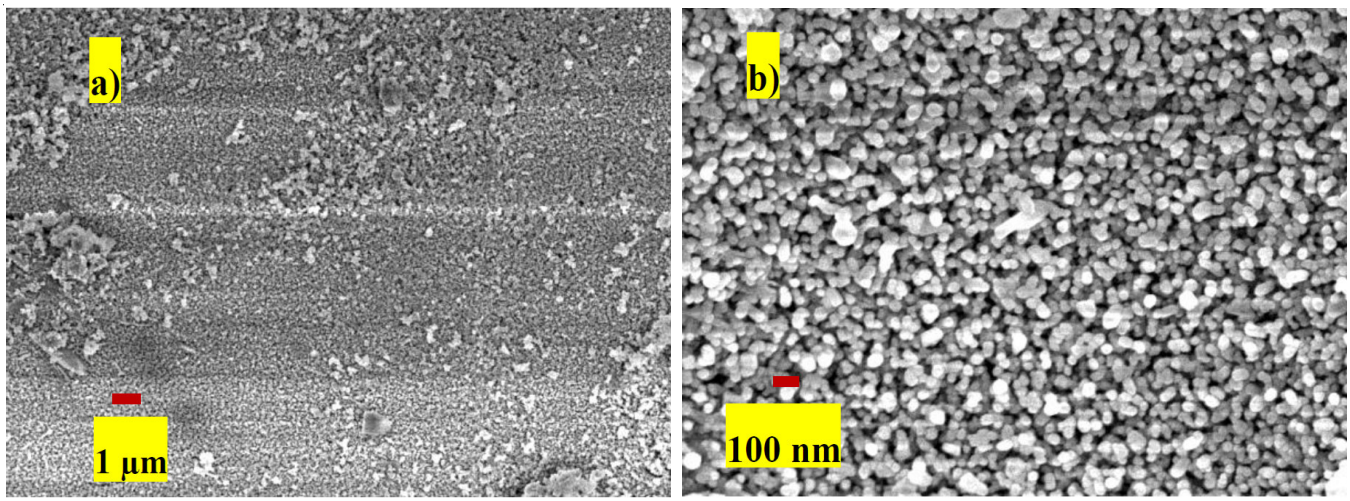

Fig. 2. SEM image of pure ZnO thin film (a) at 5000 times and (b) at 30000 times magnifications

densely packed grains which are homogenous and uniformly distributed throughout the film surface.

SEM images of a 5% Cu-5% N-ZnO thin film at various magnifications are shown in Fig. 3. A relatively denser, coral-like and smoother surface is observed compared to the previous undoped thin films. These images indicated that the mean grain size was increased, which supported the increase in particle size given in Table-1. No large porosity or cracking has been observed on any of the film surfaces. The activity of the thin films has been significantly influenced by the size of the particles. In photocatalytic system, the catalyst dispersion, dye adsorption and light absorption can all be beneficial because of the catalyst particle's uniform and tiny size [31].

EDS study: The chemical composition of the synthesized thin films was confirmed using the SEM-guided EDS technique. The EDS spectra of 5% Cu-ZnO, 5% Cu-1% N-ZnO and 5% Cu-5% N-ZnO thin films clearly show the presence of Cu and N in addition to Zn and O in 5% Cu-5% N-ZnO films, indicating that dopant elements are occupied in the crystal structure (Fig. 4). In each case of the EDS spectra of thin films, no prominent peak of other elements was found except zinc, oxygen and doping elements, which confirms the high purity of the samples.

FTIR spectral studies: As a crosscheck of the EDS analysis and for a better study of the chemical composition and purity, the synthesized thin films were analyzed by FTIR spectroscopy. Fig. 5 depicts the FTIR spectra of the samples. Three

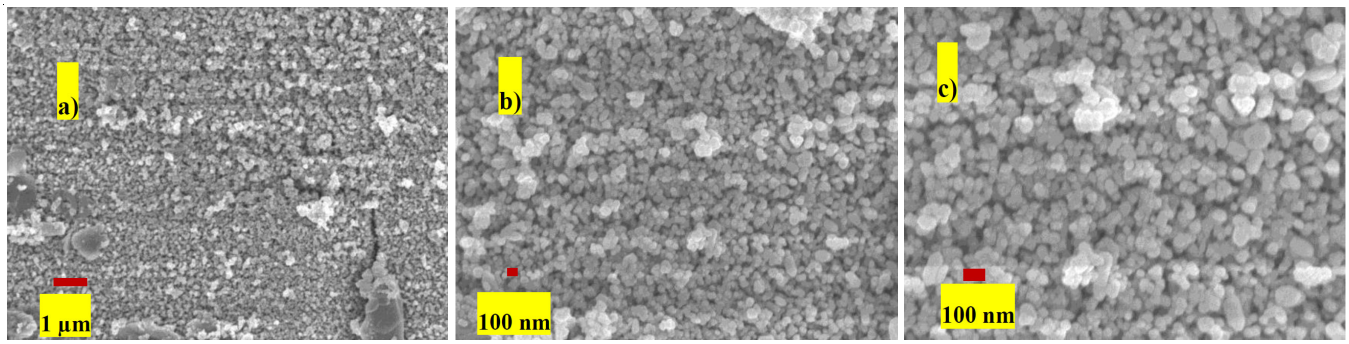

Fig. 3. SEM image of 5% Cu-5% N-ZnO thin film (a) at 5000 times and (b) at 30000 times (c) at 50000 times magnifications

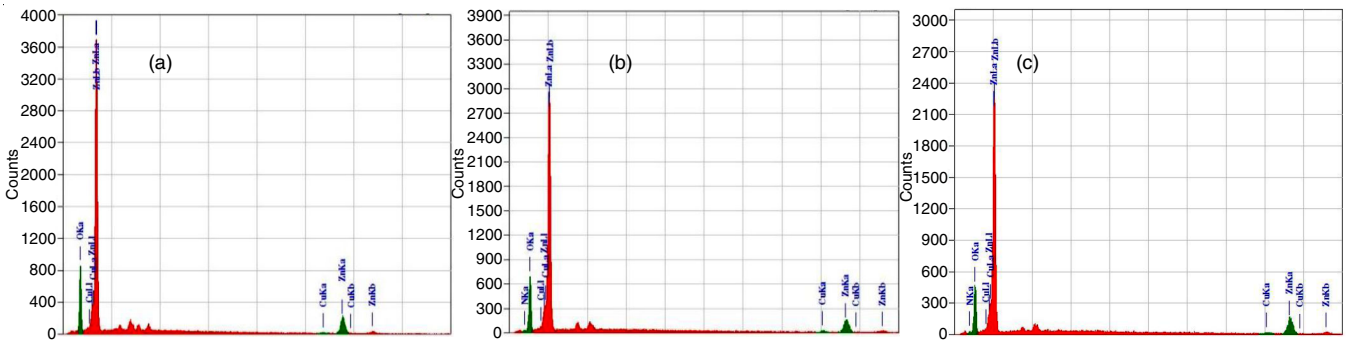

Fig. 4. EDS spectra of (a) 5% Cu-ZnO, (b) 5% Cu-1% N-ZnO and (c) 5% Cu-5% N-ZnO thin films

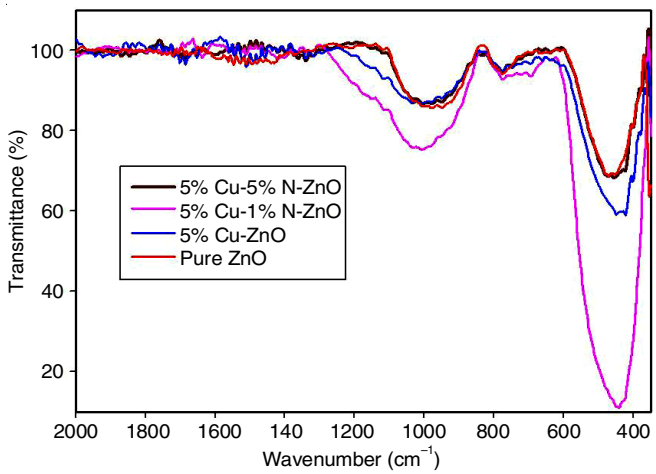

Fig. 5. FTIR spectra of Cu-N co-doped ZnO the thin films

well-defined absorption bands have been observed at around 453, 775 and 1033 cm^{-1}. The peaks at 775 and 453 cm^{-1} indicate the presence of O-Zn-O and Zn-O stretching vibrations, respectively. Another peak at 1033 cm^{-1} may appear due to the asymmetric stretching vibration of Zn-O-Zn [21-24,38,53-55]. All the peaks indicate the formation of ZnO.

UV-visible absorption spectra: The UV-visible absorption spectra of the synthesized thin films are shown in Fig. 6. All the photocatalysts show similar UV-visible absorption spectra; however, as the percentage of dopant was increased, the absorption within the visible range also increased. It suggests that as the doping percentage increases, the band gap narrows and optical absorbance increases in the visible region.

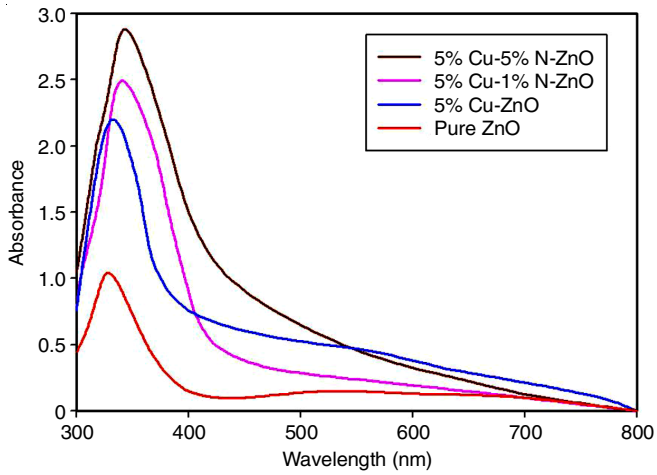

Fig. 6. UV-visible absorption spectra of Cu-N-ZnO thin films. The data shown are for samples with variable composition

The band gap of the samples was calculated by eqn. 5 and it was observed that the band gap decreases as a result of the shifting of absorption peaks to a higher wavelength (Table-2). Every sample exhibits a strong absorption in the UV and visible regions.

$$E_g = \frac{1243}{\lambda} \quad (5)$$

where, E_g is the band gap and λ is the cut off wavelength (nm) of each UV-Visible spectrum. The higher visible light absorption and the lowering band gap would facilitate better photocatalytic performance within the range of visible light by the 5% Cu-5% N-ZnO than other thin films.

TABLE-2
ESTIMATED BAND GAP OF THE THIN FILMS

Sample	Band gap (eV)
Pure ZnO	3.36
5% Cu-ZnO	3.18
5% Cu-1% N-ZnO	2.96
5% Cu-5% N-ZnO	2.89

PL spectral studies: Fig. 7 represents the PL spectra of different thin films. All the PL spectra show a similar pattern, with two emission bands in the visible range. The samples demonstrate a strong emission peak at 425 nm and a shoulder peak is also observed at 405 nm in the visible range. There is a noticeable variation in the intensity between the ZnO materials; those were doped and those were not. The decreasing PL intensity denotes longer charge separation and effective charge transport without charge carrier recombination [17]. The 5% Cu-5% N-ZnO film exhibits the lowest PL intensity, indicating more efficient charge separation and reduced recombination within the film, even though its band gap is smaller than that of pure ZnO.

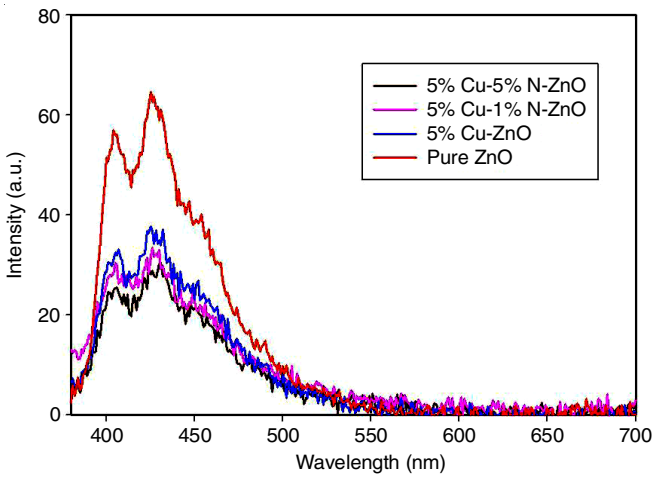

Fig. 7. PL spectra of Cu-N-ZnO thin films. The data shown are for samples with variable composition

Evaluation of photocatalytic activity: Under visible light, pure ZnO, Cu-doped ZnO and Cu and N-co-doped ZnO thin films were tested for photocatalytic activity by decomposing methylene blue (MB), a common dye pollutant. For better analysis of only photocatalysis, the adsorption by glass substrate and the photolysis of MB dye were ruled out by carrying out photolysis of MB dye in the presence of bare glass substrate at an identical condition. An insignificant change in the MB concentration was observed after 240 min of visible light irradiation on the reaction. So, the self-photolysis of MB dye and adsorption by glass substrates were neglected in all the experiments. Fig. 8 shows the comparison of the degradation efficiency of the thin films under visible light irradiation. The efficiencies were 19.4%, 27.38%, 35.56%, and 54.55% for pure ZnO, 5% Cu-ZnO, 5% Cu-1% N-ZnO, and 5% Cu-5%

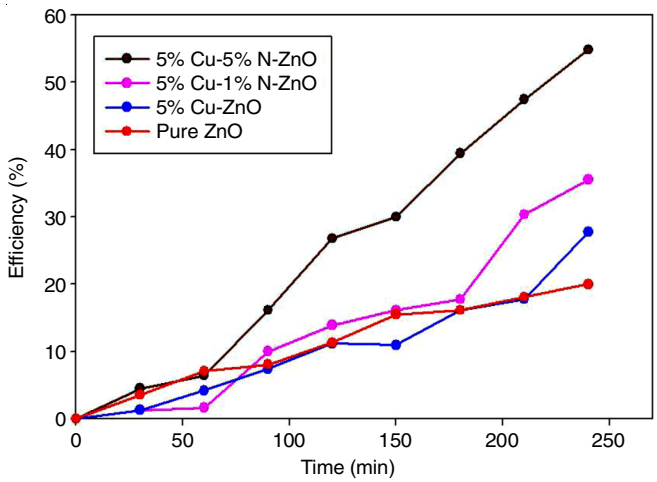

Fig. 8. Comparison of degradation efficiency of Cu-N-ZnO samples in visible light irradiation. The remarkable effect of Cu and N codoping is evident. 5% Cu-5% N-ZnO showed the highest degradation efficiency of 54.55%

N-ZnO thin films, respectively. Thin films of 5% Cu-5% N-ZnO showed the highest degradation efficiency of 54.55%.

Kinetics studies: The rate of the reaction and correlation of the degradation with both kinetic models were calculated by eqns. 2 and 3, and the results are shown in Table-3. Fig. 9 shows the correlation of the degradation study with the zero-order and first-order kinetics.

The first-order kinetics of the photocatalytic degradation of methylene blue dye are well suited, which indicates that the degradation depends on the amount of energy supplied and that the photocatalytic degradation of the dye molecules occurs at the catalytic surface of composite film [43]. The rate of degradation gradually increases with the addition of a dopant. In case of 5% Cu-5% N ZnO, the rate increased by about 62% compared to pure ZnO for zero-order kinetics, whereas in case of first-order kinetics, it was 68.70% faster than pure ZnO.

Antibacterial activity: The nanocomposite thin films were tested for their ability to inhibit *E. coli* growth. Fig. 10 illustrates the decrease in the viable count of *E. coli* on the nanocomposite thin films under visible light irradiation. A bar diagram of antibacterial efficiency is depicted in Fig. 11, which shows the comparison between the numbers of *E. coli* colonies that survived in the presence of samples exposed to 1 h of visible light irradiation and identical solutions in a dark condition.

In addition, the efficiency of the thin films in comparison to both the blank and light or dark situations is presented in Table-4. It is clear that composite films containing 5% Cu-5% N-ZnO composite films exhibited a significant reduction of *E. coli*. This could be caused by different reactive oxygen species (O^{2-}, OH^-, H_2O_2, *etc.*) which are produced by visible light irradiation on the photocatalyst. Under the effect of such reactive species, lipid peroxidation may cause *E. coli* cell death by disruption of the cell membrane structure [56,57]. Compared to the dark, 62% less bacteria could survive in the presence of visible light which exceeded ZnO by 23%.

Conclusion

The advantageous copper and nitrogen-co-doping approach to enhance the photocatalytic and antibacterial activity of ZnO has been demonstrated. Nanostructured ZnO, Cu-doped ZnO, and Cu and N-co-doped ZnO thin film photocatalysts were successfully synthesized by the low-cost sol-gel drop coating

TABLE-3
THE PHOTOCATALYTIC EFFICIENCY AND THE ANALYSIS OF THE ZERO ORDER AND FIRST ORDER KINETICS

Name of sample	Photocatalytic efficiency (%)	Zero order rate of reaction, K_0 (min^{-1})	First order rate of reaction, K_1 (min^{-1})	Regression coefficient, r^2 (zero order)	Regression coefficient, r^2 (first order)
5% Cu-5% N-ZnO	54.55	0.000500	0.0013	0.9854	0.9641
5% Cu-1% N-ZnO	35.56	0.000303	0.00068	0.9359	0.9113
Cu ZnO	27.38	0.000221	0.00047	0.9387	0.9140
ZnO	19.4	0.000190	0.00041	0.9799	0.9845

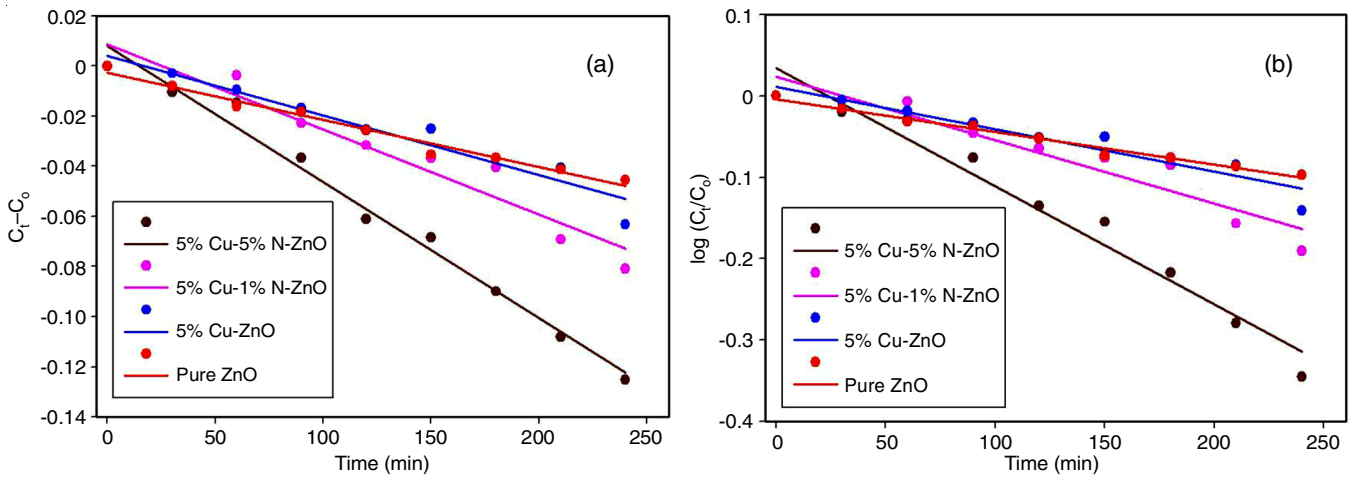

Fig. 9. Kinetics study of the photocatalytic dye degradation (a) ($C_t - C_o$) *vs.* time plot for zero order kinetics study and (b) log (C_t/C_o) *vs.* time plot for first order kinetics study kinetics study

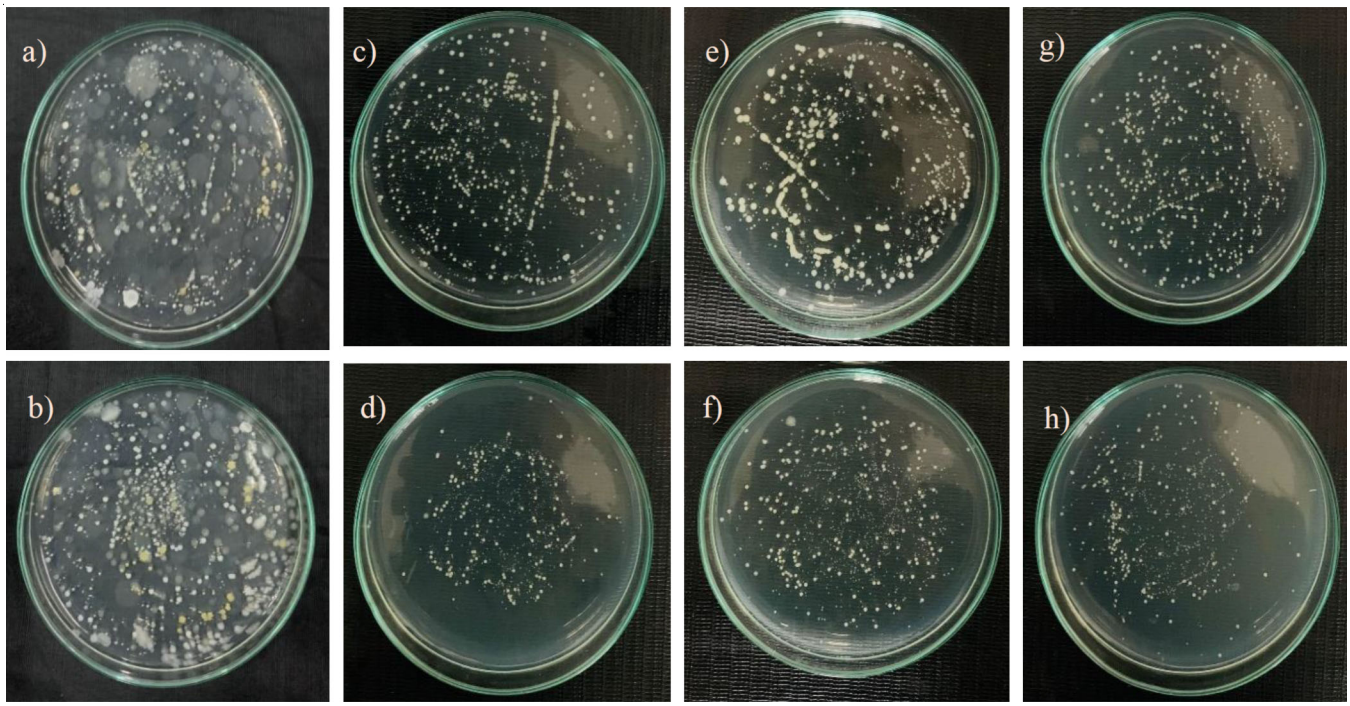

Fig. 10. Colony forming units (CFUs) of *E. coli* in various condition (a) blank (dark), (b) blank (light), (c) ZnO (dark), (d) ZnO (light), (e) 5% Cu-ZnO (dark), (f) 5% Cu-ZnO (light), (g) 5% Cu-5% N-ZnO (dark), (h) 5% Cu-5% N-ZnO (light)

TABLE-4
NUMBER OF SURVIVED COLONIES IN DARK AND LIGHT FOR VARIOUS SAMPLE

Sample	Dark	Light	Efficiency compared to blank (light) (%)	Efficiency compared to their Dark and light condition (%)
Blank	880	850	0	3.4
Pure ZnO	277	144	83	48
5% Cu-ZnO	305	127	85	58
5% Cu-1% N-ZnO	410	168	80	59
5% Cu-5% N-ZnO	475	178	79	63

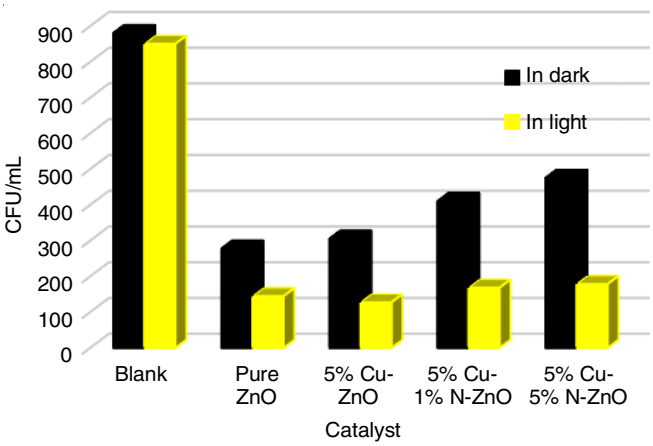

Fig. 11. Antibacterial efficiency of ZnO, 5% Cu-ZnO, 5% Cu-1% N-ZnO, 5% Cu-5% N-ZnO at dark and in presence of light

method. A wide variety of characterization techniques, such as XRD, SEM, EDS, FTIR, PL and UV-visible absorption spectroscopic methods, were performed to characterize the morphological, optical and structural characteristics of the samples. A high-crystalline nano-structured wurtzite phase of ZnO and the increasing surface area by doping were confirmed by XRD and SEM analysis. EDS spectra revealed the presence of Cu and N as the doping elements and ensured the high purity of the samples, while the presence of the Zn-O bond was confirmed by FTIR analysis. All the samples showed good optical properties through PL and UV-Visible absorption spectroscopy. Further, the Cu-N co-doped ZnO showed significant PL characteristics, having longer charge separation and high charge transport without recombination. This degradation process showed a strong correlation with first-order kinetics. Co-doping of Cu and N enhanced the photocatalytic efficiency of the samples by narrowing the band gap and reducing the rate of recombination. The samples showed the efficient antibacterial activity under visible light irradiation, while 5% Cu-5% N ZnO showed the best bacterial inactivation in the presence of visible light. It can be concluded that the 5% Cu-5% N ZnO nanomaterial could be a promising material for the photocatalytic degradation of commercial dye as well as an antimicrobial agent.

ACKNOWLEDGEMENTS

The study was supported by funding from the following sources: University Grants Commission (Projct ID: Rasayonik

Biggan Upo-Sakha 2022-2023/22) (Bangladesh), Ministry of Education, Ministry of Science & Technology, Department of Chemistry and the University Research Center (Project ID: PS/2023/1/05) of Shahjalal University of Science and Technology in Bangladesh.

CONFLICT OF INTEREST

The authors declare that there is no conflict of interests regarding the publication of this article.

REFERENCES

1. R. Yan, T. Takahashi, H. Zeng, T. Hosomi, M. Kanai, K. Nagashima, G. Zhang and T. Yanagida, *ACS Appl. Electron. Mater.*, **3**, 2925 (2021); https://doi.org/10.1021/acsaelm.1c00428
2. J.L. Yang, S.J. An, W.I. Park, G.C. Yi and W. Choi, *Adv. Mater.*, **16**, 1661 (2004); https://doi.org/10.1002/adma.200306673
3. X. Yang, A. Wolcott, G. Wang, A. Sobo, R.C. Fitzmorris, F. Qian, J.Z. Zhang and Y. Li, *Nano Lett.*, **9**, 2331 (2009); https://doi.org/10.1021/nl900772q
4. N. Kouklin, *Adv. Mater.*, **20**, 2190 (2008); https://doi.org/10.1002/adma.200701071
5. C.X. Kronawitter, Z. Ma, D. Liu, S.S. Mao and B.R. Antoun, *Adv. Energy Mater.*, **2**, 52 (2012); https://doi.org/10.1002/aenm.201100425
6. Ü. Ozgur, D. Hofstetter and H. Morkoç, *Proc. IEEE*, **98**, 1255 (2010); https://doi.org/10.1109/JPROC.2010.2044550
7. J. Zhong, J. Li, X. He, J. Zeng, Y. Lu, W. Hu and K. Lin, *Curr. Appl. Phys.*, **12**, 998 (2012); https://doi.org/10.1016/j.cap.2012.01.003
8. R.C. Ramola, S. Negi, M. Rawat, R.C. Singh and F. Singh, *ACS Omega*, **6**, 11660 (2021); https://doi.org/10.1021/acsomega.1c00984
9. M.M. Ba-abbad, A.A.H. Kadhum, A.B. Mohamad, M.S. Takriff and K. Sopian, *Chemosphere*, **91**, 1604 (2013); https://doi.org/10.1016/j.chemosphere.2012.12.055
10. M. Elias, M.K. Amin, S.H. Firoz, M.A. Hossain, S. Akter, M.A. Hossain, M.N. Uddin and I.A. Siddiquey, *Ceram. Int.*, **43**, 84 (2017); https://doi.org/10.1016/j.ceramint.2016.09.114
11. F. Tsin, A. Thomere, A. L. Bris, S. Collin, D. Lincot and J. Rousset, *ACS Appl. Mater. Interf.*, **8**, 12298 (2016); https://doi.org/10.1021/acsami.6b02998
12. A. Jiamprasertboon, S.C. Dixon, S. Sathasivam, M.J. Powell, Y. Lu, T. Siritanon and C.J. Carmalt, *ACS Appl. Electron. Mater.*, **1**, 1408 (2019); https://doi.org/10.1021/acsaelm.9b00190
13. A. Omidi, A. Habibi-yangjeh and M. Pirhashemi, *Appl. Surf. Sci.*, **276**, 468 (2013); https://doi.org/10.1016/j.apsusc.2013.03.118
14. H. Sun, S. Liu, S. Liu and S. Wang, *Appl. Catal. B*, **146**, 162 (2014); https://doi.org/10.1016/j.apcatb.2013.03.027
15. T. Lv, L. Pan, X. Liu and Z. Sun, *Catal. Sci. Technol.*, **2**, 2297 (2012); https://doi.org/10.1039/c2cy20023f
16. M. Ahmad, E. Ahmed, Y. Zhang, N.R. Khalid, J. Xu, M. Ullah and Z. Hong, *Curr. Appl. Phys.*, **13**, 697 (2013); https://doi.org/10.1016/j.cap.2012.11.008
17. R. Gupta, N.K.R. Eswar, J.M. Modak and G. Madras, *RSC Advances*, **6**, 85675 (2016); https://doi.org/10.1039/C6RA16739J
18. B. Soltabayev, G. Yergaliuly, A. Ajjaq, A. Beldeubayev, Z. Bakenov, S. Acar and A. Mentbayeva, *ACS Appl. Mater. Interfaces*, **14**, 41555 (2022); https://doi.org/10.1021/acsami.2c10055
19. M. Salem, S. Akir, T. Ghrib, K. Daoudi and M. Gaidi, *J. Alloys Compd.*, **685**, 107 (2016); https://doi.org/10.1016/j.jallcom.2016.05.254
20. R. Saleh and N.F. Djaja, *Superlattices Microstruct.*, **74**, 217 (2014); https://doi.org/10.1016/j.spmi.2014.06.013
21. M.S. Abdel-wahab, A. Jilani, I.S. Yahia and A.A. Al-Ghamdi, *Superlattices Microstruct.*, **94**, 108 (2016); https://doi.org/10.1016/j.spmi.2016.03.043
22. S. Rajeh, A. Barhoumi, A. Mhamdi, G. Leroy, B. Duponchel, M. Amlouk and S. Guermazi, *Bull. Mater. Sci.*, **39**, 177 (2016); https://doi.org/10.1007/s12034-015-1132-4
23. M. Karunakaran, R. Chandramohan, S. Balamurali, S. Gomathi, K. Kabila and T. Mahalingam, *Int. J. Thin Film Sci. Technol.*, **3**, 61 (2014); https://doi.org/10.12785/ijtfst/030206
24. V. Rajendar, T. Dayakar, K. Shobhan, I. Srikanth and K.V. Rao, *Superlattices Microstruct.*, **75**, 551 (2014); https://doi.org/10.1016/j.spmi.2014.07.049
25. T. Saidani, M. Zaabat, M.S. Aida and B. Boudine, *Superlattices Microstruct.*, **88**, 315 (2015); https://doi.org/10.1016/j.spmi.2015.09.029
26. S. Yang, Y. Zhang and D. Mo, *Thin Solid Films*, **571**, 605 (2014); https://doi.org/10.1016/j.tsf.2014.02.097
27. S.S. Zahirullah, J.J. Prince and P.F.H. Inbaraj, *Mater. Technol.*, **32**, 755 (2017); https://doi.org/10.1080/10667857.2017.1351656
28. S. Thakur, N. Sharma, A. Varkia and J. Kumar, *Adv. Appl. Sci. Res.*, **5**, 18 (2014).
29. K. Kim, *J. Korean Phys. Soc.*, **57**, 264 (2010); https://doi.org/10.3938/jkps.57.264
30. W.H. Kim and J.Y. Son, *Mater. Lett.*, **133**, 101 (2014); https://doi.org/10.1016/j.matlet.2014.06.180
31. H.F. Moafi, M.A. Zanjanchi and A.F. Shojaie, *Mater. Chem. Phys.*, **139**, 856 (2013); https://doi.org/10.1016/j.matchemphys.2013.02.044
32. E. Isbilir, Z. Serbetci and M. Soylu, *Superlattices Microstruct.*, **67**, 144 (2014); https://doi.org/10.1016/j.spmi.2013.12.017
33. J. Park, G. Park, H.J. Ko and J.S. Ha, *Ceram. Int.*, **40**, 16281 (2014); https://doi.org/10.1016/j.ceramint.2014.07.065
34. P.V. Adhyapak, S.P. Meshram, A.A. Pawar, D.P. Amalnerkar, U.P. Mulik and I.S. Mulla, *Ceram. Int.*, **40**, 12105 (2014); https://doi.org/10.1016/j.ceramint.2014.04.050
35. M. Hjiri, R. Dhahri, L. El Mir, A. Bonavita, N. Donato, S.G. Leonardi and G. Neri, *J. Alloys Compd.*, **634**, 187 (2015); https://doi.org/10.1016/j.jallcom.2015.02.083
36. X. Wang, X. Huang, Z.M. Wong, A. Suwardi, Y. Zheng, F. Wei, S. Wang, T.L. Tan, G. Wu, Q. Zhu, H. Tanoto, K.S. Ong, S.-W. Yang, A.Q. Yan and J. Xu, *ACS Appl. Nano Mater.*, **5**, 8631 (2022); https://doi.org/10.1021/acsanm.2c02159
37. A.C. Badgujar, B.S. Yadav, G.K. Jha and S.R. Dhage, *ACS Omega*, **7**, 14203 (2022); https://doi.org/10.1021/acsomega.2c00830
38. R. Kumar, A. Umar, G. Kumar, M.S. Akhtar, Y. Wang and S.H. Kim, *Ceram. Int.*, **41**, 7773 (2015); https://doi.org/10.1016/j.ceramint.2015.02.110
39. M. Elias, M.N. Uddin, M.A. Hossain, J.K. Saha, I.A. Siddiquey, D.R. Sarkar, Z.R. Diba, J. Uddin, M.H.R. Choudhury and S.H. Firoz, *Int. J. Hydrogen Energy*, **44**, 20068 (2019); https://doi.org/10.1016/j.ijhydene.2019.06.056
40. G.N. Dar, A. Umar, S.A. Zaidi, A.A. Ibrahim, M. Abaker, S. Baskoutas and M.S. Al-assiri, *Sens. Actuators B Chem.*, **173**, 72 (2012); https://doi.org/10.1016/j.snb.2012.06.001
41. M. Faisal, A.A. Ismail, A.A. Ibrahim, H. Bouzid and S.A. Al-Sayari, *Chem. Eng. J.*, **229**, 225 (2013); https://doi.org/10.1016/j.cej.2013.06.004
42. L.G. Devi and R. Kavitha, *Appl. Catal. B*, **140-141**, 559 (2013); https://doi.org/10.1016/j.apcatb.2013.04.035
43. C.S. Chen, X.D. Xie, T.G. Liu, L.W. Lin, J.C. Kuang, X.L. Xie, L.J. Lu and S.Y. Cao, *J. Nanopart. Res.*, **14**, 817 (2012); https://doi.org/10.1007/s11051-012-0817-5
44. Y. Yan, M. Al-Jassim and S.-H. Wei, *Appl. Phys. Lett.*, **89**, 181912 (2006); https://doi.org/10.1063/1.2378404
45. M. Ahmad, E. Ahmed, Z.L. Hong, X.L. Jiao, T. Abbas and N.R. Khalid, *Appl. Surf. Sci.*, **285**, 702 (2013); https://doi.org/10.1016/j.apsusc.2013.08.114

46. G. Liu, L. Wang, H.G. Yang, H.-M. Cheng and G.Q. (Max) Lu, *J. Mater. Chem.*, **20**, 831 (2010); https://doi.org/10.1039/B909930A
47. C.W. Dunnill and I.P. Parkin, *Dalton Trans.*, **40**, 1635 (2011); https://doi.org/10.1039/C0DT00494D
48. F. Peng, L. Cai, H. Yu, H. Wang and J. Yang, *J. Solid State Chem.*, **181**, 130 (2008); https://doi.org/10.1016/j.jssc.2007.11.012
49. M.N. Uddin, M.S. Islam, M.M.R. Mazumder, M.A. Hossain, M. Elias, I.A. Siddiquey, M.A.B.H. Susan, D.K. Saha, M.M. Rahman, A.M. Asiri and S. Hayami, *J. Incl. Phenom. Macrocycl. Chem.*, **82**, 229 (2015); https://doi.org/10.1007/s10847-015-0510-2
50. J. Lv, W. Gong, K. Huang, J. Zhu, F. Meng, X. Song and Z. Sun, *Superlattices Microstruct.*, **50**, 98 (2011); https://doi.org/10.1016/j.spmi.2011.05.003
51. B. Subash, B. Krishnakumar, M. Swaminathan and M. Shanthi, *Spectrochim. Acta A Mol. Biomol. Spectrosc.*, **105**, 314 (2013); https://doi.org/10.1016/j.saa.2012.12.035
52. B.D. Cullity, *Add. Wes.*, **1956**, 51 (1978).
53. R. Kumar, O. Al-Dossary, G. Kumar and A. Umar, *Nano-Micro Lett.*, **7**, 97 (2015); https://doi.org/10.1007/s40820-014-0023-3
54. R. Kumar, G. Kumar and A. Umar, *Nanosci. Nanotechnol. Lett.*, **6**, 631 (2014); https://doi.org/10.1166/nnl.2014.1879
55. O. Yayapao, S. Thongtem, A. Phuruangrat and T. Thongtem, *Ceram. Int.*, **39**, 563 (2013); https://doi.org/10.1016/j.ceramint.2012.10.136
56. P.C. Maness, S. Smolinski, D.M. Blake, Z. Huang, E.J. Wolfrum and W.A. Jacoby, *Appl. Environ. Microbiol.*, **65**, 4094 (1999); https://doi.org/10.1128/AEM.65.9.4094-4098.1999
57. M.A. Hossain, M. Elias, D.R. Sarker, Z.R. Diba, J.M. Mithun, M.A.K. Azad, I.A. Siddiquey, M.M. Rahman, J. Uddin and M.N. Uddin, *Res. Chem. Intermed.*, **44**, 2667 (2018); https://doi.org/10.1007/s11164-018-3253-z